REPORT

Geological context of the Chang'e-6 landing area and implications for sample analysis

Zongyu Yue,[1,5,*] Sheng Gou,[1] Shujuan Sun,[2,3] Wei Yang,[1] Yi Chen,[4] Yexin Wang,[2] Honglei Lin,[1] Kaichang Di,[2,5] Yangting Lin,[1] Xianhua Li,[4] and Fuyuan Wu[4]

*Correspondence: yuezy@mail.iggcas.ac.cn

Received: June 4, 2024; Accepted: June 21, 2024; Published Online: June 24, 2024; https://doi.org/10.1016/j.xinn.2024.100663

GRAPHICAL ABSTRACT

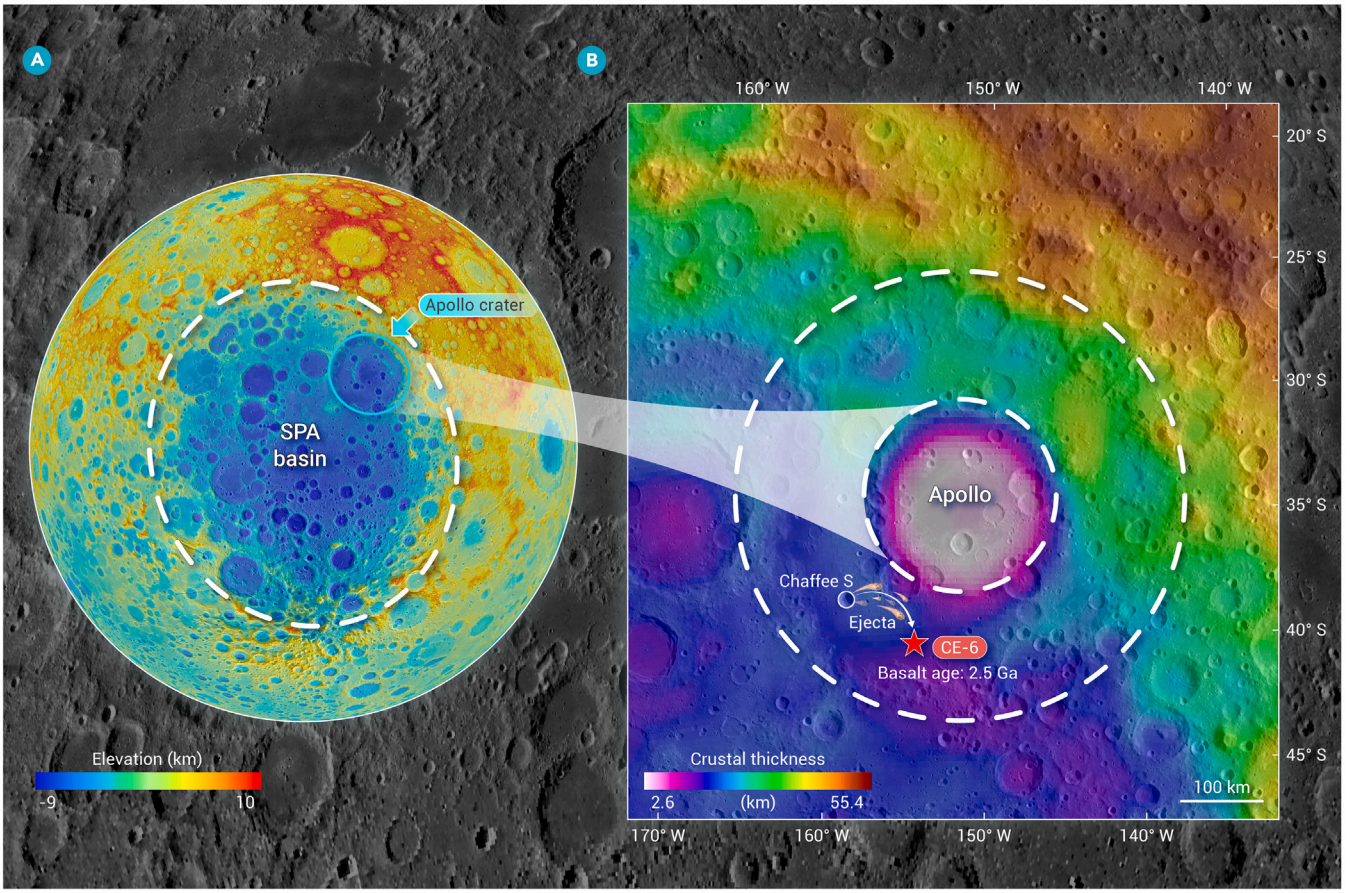

PUBLIC SUMMARY

- The model age of Chang'e-6 landing area is ~2.50 Ga.
- The ejecta from Chaffee S crater at Chang'e-6 landing site is numerically analyzed.
- Chang'e-6 samples may contain impact melt from the Apollo crater and the South Pole-Aitken basin.

REPORT

Geological context of the Chang'e-6 landing area and implications for sample analysis

Zongyu Yue,[1,5,*] Sheng Gou,[1] Shujuan Sun,[2,3] Wei Yang,[1] Yi Chen,[4] Yexin Wang,[2] Honglei Lin,[1] Kaichang Di,[2,5] Yangting Lin,[1] Xianhua Li,[4] and Fuyuan Wu[4]

[1]Key Laboratory of Earth and Planetary Physics, Institute of Geology and Geophysics, Chinese Academy of Sciences, Beijing 100029, China

[2]State Key Laboratory of Remote Sensing Science, Aerospace Information Research Institute, Chinese Academy of Sciences, Beijing 100101, China

[3]School of Architecture and Civil Engineering, Chengdu University, Chengdu 610106, China

[4]State Key Laboratory of Lithospheric Evolution, Institute of Geology and Geophysics, Chinese Academy of Sciences, Beijing 100029, China

[5]Center for Excellence in Comparative Planetology, Chinese Academy of Sciences, Hefei 230026, China

*Correspondence: yuezy@mail.iggcas.ac.cn

Received: June 4, 2024; Accepted: June 21, 2024; Published Online: June 24, 2024; https://doi.org/10.1016/j.xinn.2024.100663

Citation: Yue Z., Gou S., Sun S., et al., (2024). Geological context of the Chang'e-6 landing area and implications for sample analysis. The Innovation **5(5)**, 100663.

Research on returned samples can provide ground truth for the study of the geological evolution history of the Moon. However, previous missions all collected samples from the near side of the Moon, which is significantly different from the far side of the Moon in terms of the thickness of the lunar crust, magma activity, and composition. Therefore, the samples from the far side of the Moon are of great significance for a comprehensive understanding of the history of the Moon. China's Chang'e-6 (CE-6) probe has successfully landed on the lunar far side and will return samples in the coming days. With the precise location of the CE-6 landing site, a detailed analysis of the geological background is conducted in this research. The landing site of CE-6 is within the Apollo crater, which is inside the largest impact basin on the Moon, i.e., the South Pole-Aitken (SPA) basin. According to the numerical simulation of the formation process of the SPA basin, CE-6 landed at the edge of the SPA impact melting zone, which is presumably composed of impact melt of the lunar mantle. The Apollo crater subsequently excavated deep material again, which constitutes the basement of the CE-6 landing area. Later, erupted basalt covered these basement rocks, and they also constitute the main source of the CE-6 samples. Based on the dating method of crater size-frequency distribution, we find that the basalt is ~2.50 Ga. The CE-6 samples also possibly contain basement rocks as excavated and ejected by craters, and they can provide crucial information for our understanding of lunar geological history along with the basalt samples.

INTRODUCTION

Lunar samples are the cornerstone of lunar scientific research in that they can provide ground truth information on the origination and evolution of the Moon.[1–7] However, the previous samples returned by the six Apollo, three Luna, and Chang'e-5 (CE-5) spacecraft are all from the lunar near side. Because of the Moon's asymmetry between the near side and far side,[8–12] the samples from the far side are extremely important to analyze some fundamental questions such as the composition and structure of the lunar interior, impact history, etc. The CE-6 probe, the backup of the CE-5 mission, was launched on May 3, 2024, and successfully landed in the Apollo crater in the South Pole-Aitken (SPA) basin on the lunar far side on June 2, 2024. The precise location of the CE-6 landing site is 153.9856°W, 41.6383°S.[13] Subsequently, the lander-ascender combination is scheduled to collect ~2.0 kg of samples using a drill and a mechanical arm, and the ascender will return the samples to Earth. This is the first time humanity will be collecting lunar samples from the far side of the Moon, and a small amount of soil can effectively address many outstanding scientific problems as exemplified by the CE-5 mission.[14] For example, the radiometric measurements of CE-5 samples indicate that the Moon still had volcanic activity at ~2.0 Ga,[15,16] which was unexpectedly from a non-potassium, rare-earth elements and phosphorus (non-KREEP) mantle source[17] and not driven by abundant water in its mantle source.[3] The radiometric age of the CE-5 samples was also used to update the lunar chronology model,[18] which is important to study the impact history of the inner solar system.

One reason that CE-5 samples could spawn so many papers within a short period is that detailed analyses were conducted on the geological background,[19] impact history of the landing area,[20] and provenance of the sample[21] prior to analyzing the samples in the laboratory. These studies provided basic information in interpreting the returned samples. It is expected that the CE-6 samples will also undergo a significant amount of research work once it is returned. Therefore, a detailed analysis on the sampling area was conducted in this research, which should provide important information for the interpretation of CE-6 samples in the near future.

RESULTS

Geological background of CE-6 landing area

The landing site of CE-6 is in the south of the Apollo crater inside the SPA basin (Figure 1). The SPA basin is the largest (2,400 × 2,050 km in diameter),[22] deepest (~13 km in depth), and oldest (~4.25 Ga)[23] impact basin on the Moon,[24] and it is generally considered as having exposed the lunar mantle materials.[25–27] Using Moon Mineralogy Mapper data, Moriarty and Pieters[28] found that the central SPA compositional anomaly (SPACA) zone was characterized by elevated Ca, Fe-rich pyroxene abundance, which are most probably indicative of impact melt from the lunar mantle material. It is important to note that the SPACA is largely consistent with the continuous molten mantle material in the numerical simulations of the formation of the SPA basin.[27] The landing site of CE-6 is in the Mg-pyroxene annulus, which is dominated by abundant Mg-rich pyroxenes, but it is very close to its edge (Figure 1). This implies that the composition of the material source area beneath the CE-6 landing site may be very complex, dominated by early lunar mantle material but also including a small amount of early lunar crust. Additionally, differentiation may have occurred due to impact melting.[29]

The Apollo crater is the largest crater (~492 km in diameter)[30,31] within the SPA basin, and it provides an opportunity to assess the SPA substructure. Based on the size-frequency distribution of the superposed craters, the age of the Apollo crater has been estimated to be ~3.91–4.14 Ga.[32–34] In some studies, the Apollo crater is regarded as a peak-ring basin, and its inner peak ring has a diameter of ~247 km.[31,35,36] However, the sole inner ring is almost symmetric in topography (Figure 2A), indicating that the Apollo crater should be classified as a peak-ring crater according to Melosh.[37] There is a significant positive Bouguer gravity anomaly in the center of the Apollo crater (Figure 2B), which corresponds to the very thin lunar crust in this area (Figure 2C). With numerical simulations, Potter et al.[38] suggest that the Apollo crater straddles the SPA transient crater and modification zone. The CE-6 landing site is located on the southern edge of the Apollo crater, where the Mg-rich pyroxenes were interpreted to represent a remnant part of the SPA transient cavity.[38]

There are plenty of craters inside the Apollo crater, with various formation ages (Figure 3A), e.g., Copernican-aged Chaffee S crater, Late Imbrian-aged Dryden crater.[33] The oxide abundances[39] and Mg# of these craters and other typical geological units around the Apollo crater are shown in Figure 3. The Mg# (50.5% ± 6.6%) and oxide abundances (e.g., FeO: 16.7% ± 2.9%) of the mare basalt unit are rather different from the rest of the geological units (Figures 3B and S1), indicating a complex geological context in the Apollo crater. Due to continuous bombardment on the lunar surface, materials from other geological units are likely to have been ejected to the CE-6 landing area.

Basalt unit of CE-6 landing area

The landing site of CE-6 is located on the basalt within the Apollo crater. Figure S2 shows the distributions of clinopyroxene, orthopyroxene, olivine, feldspar,

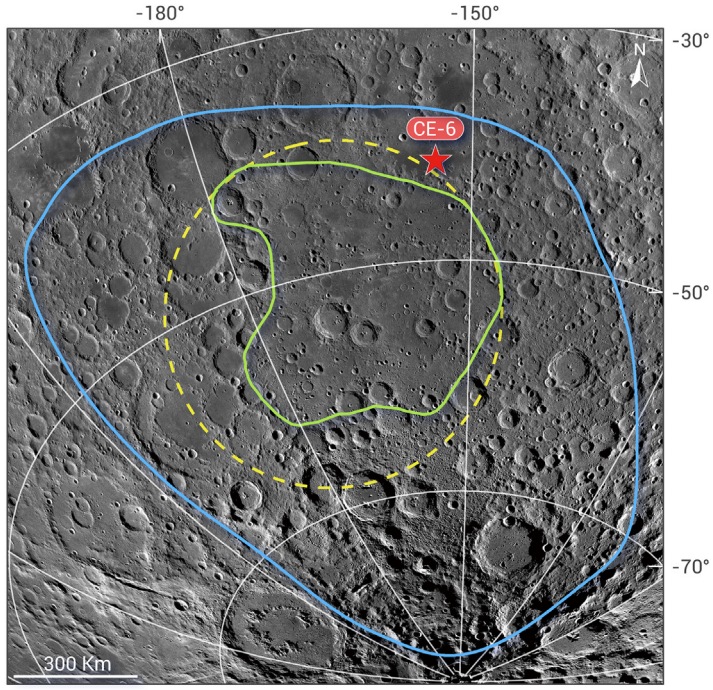

Figure 1. Location of the CE-6 landing site The green polygon represents SPACA zone characterized with elevated Ca, Fe-rich pyroxene abundance, which is largely coincident with the continuous molten material during the formation of SPA (dashed yellow line). The blue line represents the outer boundary of the Mg-rich pyroxenes area. An orthographic projection is used in this map, with the center at the SPA basin.

and FeO based on the results by Lemelin et al.[40] and TiO_2 by Sato et al.[41] Based on the spectral and compositional homogeneity,[42] the geological unit of the CE-6 landing area is delineated and further refined in a high-resolution Lunar Reconnaissance Orbiter Camera (LROC) narrow-angle camera (NAC) mosaic (Figure 4A). Areas that have abnormal mineral compositions or clustered secondary craters have been eliminated from this geologic unit. The abundances (mean ± variance) of clinopyroxene (29.4% ± 9.1%), orthopyroxene (26.0% ± 6.7%), olivine (8.9% ± 4.2%), plagioclase (35.8% ± 5.1%), FeO (17.9% ± 1.0%), and TiO_2 (6.1% ± 1.4%) in the geologic unit have been measured. According to the classification criteria by Giguere et al.,[43] the CE-6 landing area is an intermediate-titanium basalt.

Figure 4A also shows the craters >100 m (~33 pixels) in diameter mapped in this research. There are 3,346 craters in total, and the maximum diameter is about 1.7 km (Crater Data: https://zenodo.org/doi/10.5281/zenodo.11425687). To examine whether the established geological boundary has a significant effect on the statistical results of impact craters, we gradually reduced the boundary inward by 2.5, 5.0, and 7.5 km in sequence (Figure S3) and then compared the size-frequency distributions of the impact craters. Figure S4A shows the results indicating that the size-frequency distribution of craters smaller than ~700 m in diameter is almost unaffected by the geological boundaries. Meanwhile, the analysis of the completeness diameter of the mapped craters is 270 m (Figure 4B) based on the method by Robbins et al.[44] Figure 4C shows the surface dating results according to the size-frequency distribution of the mapped craters, in which the crater production function by Neukum et al.[45] and the chronology function by Yue et al.[18] are used. Based on the size-frequency distributions of the craters between 270 and 700 m in diameter, the absolute model age is $2.50^{+0.078}_{-0.080}$ Ga and the $N(1)$ value is 1.92 km^{-2} according to the method of Poisson timing analysis,[46] which is independent of the crater binning width. In addition, the clustering analysis with the method of mean 2nd-closest neighbor distance[47] shows that craters larger than 250 m in diameter are randomly distributed (Figure 4C), i.e., the dating result is not

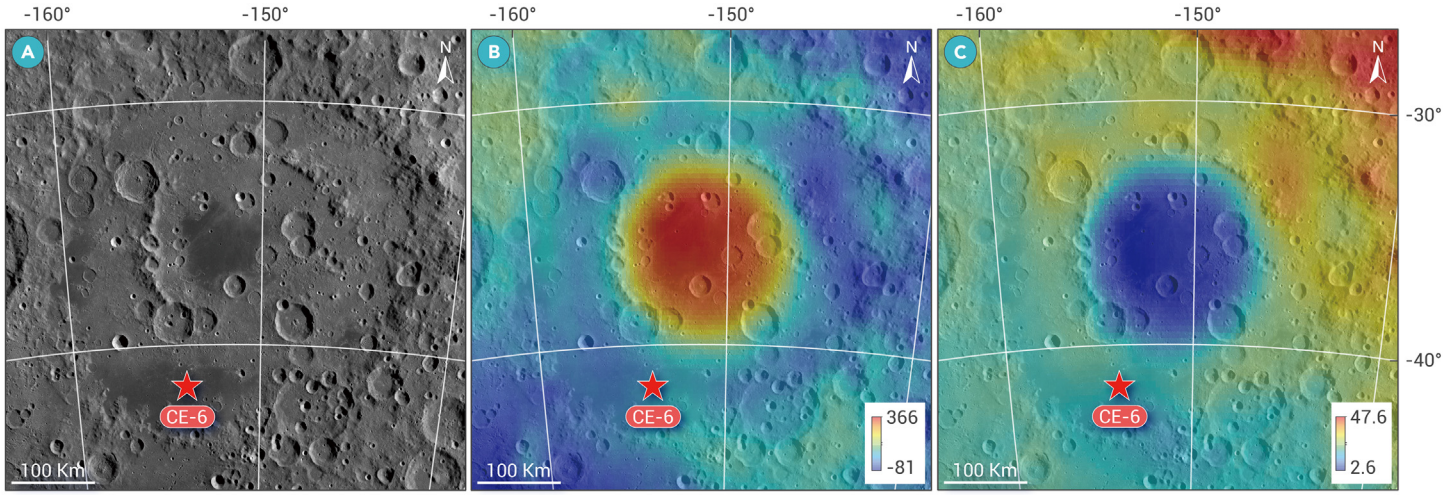

Figure 2. The Apollo crater and CE-6 landing site (A) The CE-6 landing site is located in the southern Apollo crater. (B) Bouger gravity anomaly map (unit: mgal). (C) Lunar crust thickness (unit: km). Orthographic projections are used in (A)–(C), with the centers at the Apollo crater.

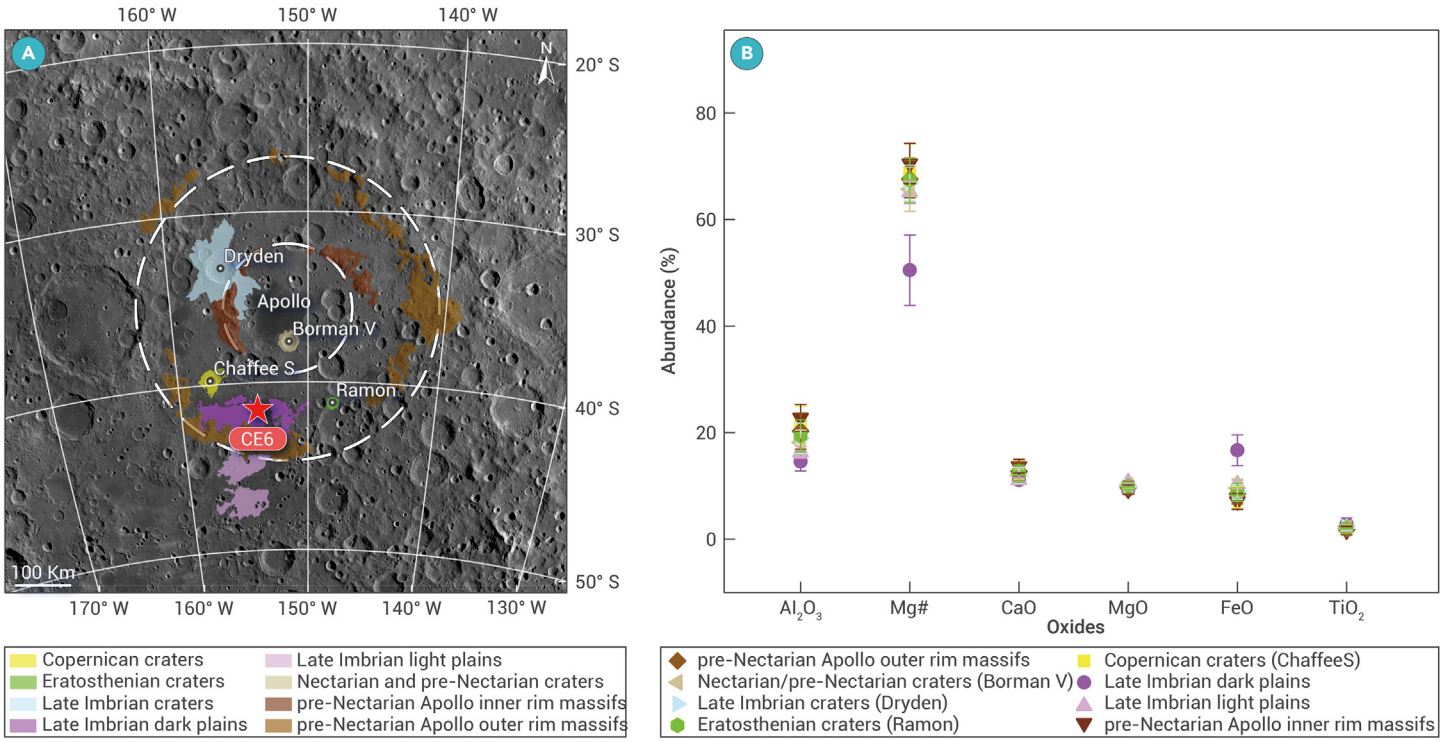

Figure 3. Typical geological units and geochemistry analysis around the Apollo crater (A) Typical geological units around Apollo crater. (B) Oxide abundances and Mg# of these geological units. An orthographic projection is used in (A), with the center at the Apollo crater.

affected by secondary craters. We also conducted dating analysis on the impact craters in different counting areas in Figure S3, and the maximum deviation among these results is ~8% (Figure S4). The deviation should be attributed to the randomness of the distribution of impact craters, and the dating result from the entire counting area should be with a smaller uncertainty. The dating result is younger than that by Qian et al.,[48] which is most probably because a much larger counting area is included therein.

Exotic material of the CE-6 samples

A total of 253 Copernican impact craters have been discovered on the surface of the Moon (Figure 5), and their ejecta may be included in the returned CE-6 samples. Based on the empirical formula for the thickness of crater ejecta,[49] we evaluated the ejecta thickness of these young craters in the CE-6 landing site. The result indicates that the total ejecta thickness from these craters is ~21.5 cm, while the ejecta from the Chaffee S crater (~20 km in diameter) is ~16.2 cm. This analysis indicates that there is a high probability that the CE-6 samples include ejecta from Chaffee S crater, as recently suggested by Jia et al.[50] Since the Chaffee S crater is located in an area rich in noritic materials[51] that are probably from the impact melt of the Apollo crater, the CE-6 samples may contain impact melt produced during the formation of the Apollo crater. If this is the case, then the CE-6 samples will provide crucial evidence for determining the age of the Apollo crater.

To analyze the initial depth of the ejecta from the Chaffee S crater, we carried out a numerical simulation of its formation (Figure S5; Table S1). Figure 6 shows the ejected distance for the original material during the formation of the Chaffee S crater, in which the diameter and velocity of the projectile are set as 1.6 km and 11 km/s, respectively. Because this is a numerical simulation of a vertical impact, the material beneath the impact point will not be excavated. The results show that the ejected distance of the original target exhibits an approximately concentric ring-shaped distribution. The initial locations of the material that could be ejected to the CE-6 landing site nearby are indicated by the black dashed line. The result shows that the ejected material may be from different depths, with the maximum depth of the source material being about 1.5 km.

The Vavilov crater (Figure 5) ranks second in terms of the thickness of ejecta (~1.7 cm) at the CE-6 landing site. This crater is located on the lunar highlands, implying that the CE-6 samples may contain a very small amount of lunar highland material. The remaining Copernican craters have very little ejecta at the CE-6 landing site. In addition, some Eratosthenian craters may also have ejected material to the CE-6 landing site. Although the ejecta may be covered by later Copernican craters' ejecta, or even by basalt if they are older than the CE-6 basalt, the later impact excavation processes in the region may have excavated the older ejecta to the surface, which were then coincidentally collected by the CE-6 mission. We analyzed the ejecta thickness of the Eratosthenian craters within the Apollo crater, as shown in Figure S6. The results indicate that the total thickness of the ejecta at the CE-6 landing site from these impact craters is ~40.6 cm. This further increases the probability that the CE-6 samples contain impact melt from the Apollo crater. Similarly, we analyzed the thickness of ejecta from 21 Eratosthenian impact craters within the SPA basin at the CE-6 landing site (Figure S7). The results show that the total thickness of the ejecta at the CE-6 landing site is about 57.3 cm, while the ejecta thickness from the White crater (42.34 km in diameter) is ~49.3 cm. Since the White crater is within the SPACA, the CE-6 samples may contain impact melt formed during SPA basin formation.

DISCUSSION

Significant issues to be addressed

The scientific research on CE-6 samples is expected to provide key information on the following problems: (1) the age of the SPA basin. The CE-6 mission is expected to collect impact melt formed during the formation of the SPA basin to accurately obtain its age. (2) The age of the Apollo crater. There is a high probability that the CE-6 samples contain impact melt from the Apollo crater. The radiometric ages of the SPA basin and Apollo crater can greatly promote the study of the early lunar impact flux. (3) The major mineral composition of the lunar mantle. The formation process of the SPA basin exposes lunar mantle material, but due to the lack of observation of large-scale olivine, some studies speculate that the main component of the lunar mantle is low-calcium pyroxene rather than olivine like the Earth.[26] Geochemical analysis of the samples will help to uncover this mystery. (4) The lunar impact flux function. With the radiometric ages of the samples and crater size-frequency distribution of the areas represented by the samples, the lunar impact flux function can be further optimized. This is the only sample from the far side of the Moon, and it is of great significance for studying the distribution of lunar impact fluxes. (5) The volcanic eruption inside the SPA basin. Current research shows that the thickness of the lunar crust inside the SPA basin is small, but there is no large-scale basalt exposure inside. Geochemical research on CE-6 samples,

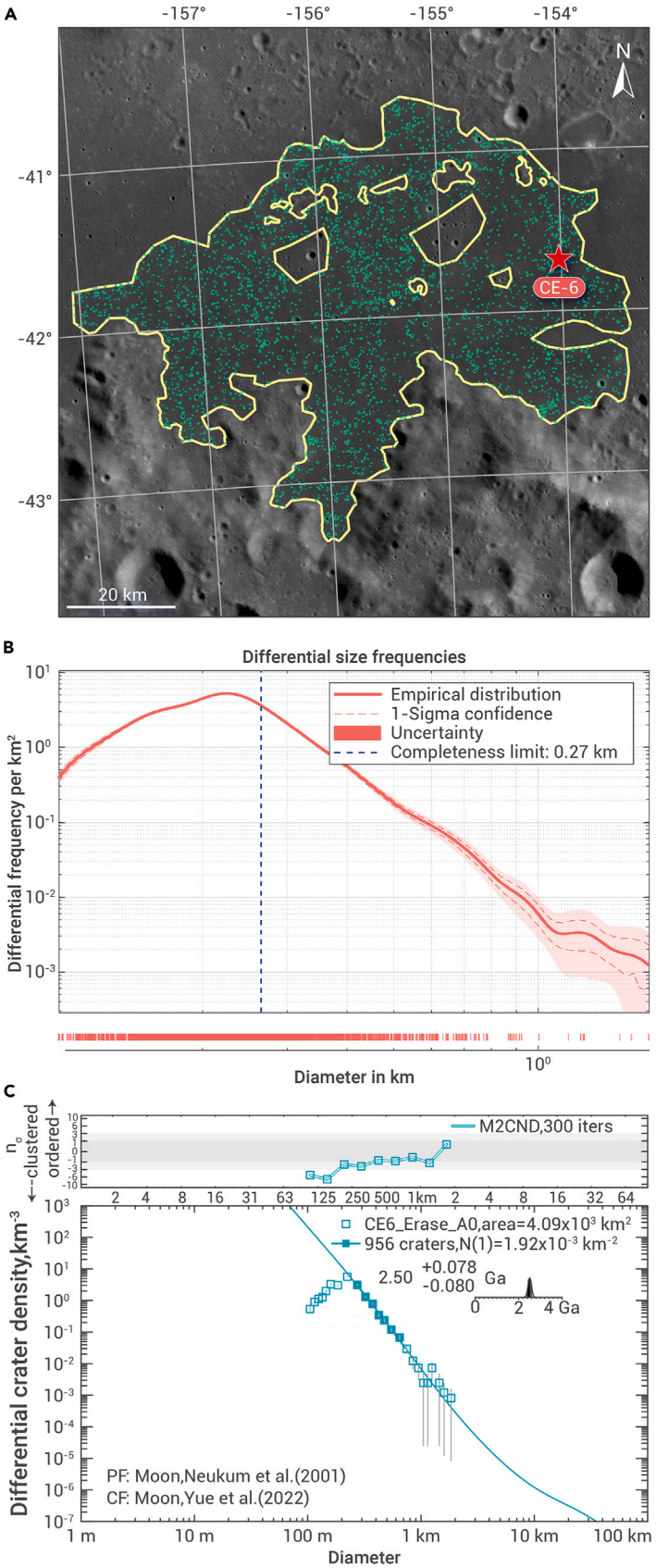

Figure 4. Geological unit of the CE-6 landing area and crater analysis therein (A) Boundary of the geological unit and mapped crater. (B) Crater completeness diameter analysis. (C) Dating result of CE-6 landing area with the mapped craters. Orthographic projections are used in (A) and (B), with the centers at the CE-6 landing site.

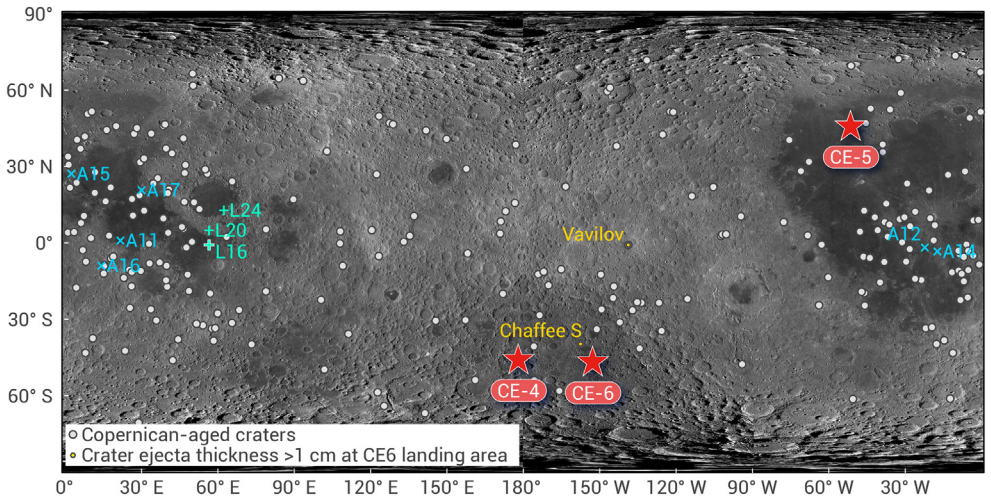

Figure 5. Potential source craters for the exotic material in the CE-6 sample The white spots are the Copernican craters, and the two yellow spots are the most likely craters responsible for the exotic materials in CE-6 sample. The sampling sites are also shown in the figure (A, Apollo; L, Luna). Note that the lunar far side is in the center. Equirectangular projection is used in this map.

especially a comparison with the chemical composition of basalt on the near side of the Moon, will help solve this problem. (6) The asymmetry of the Moon. By combining the above analyses, the long-standing issue of the asymmetry between the near and far sides of the Moon on crust thickness, volcanic activity, and internal structure, which has perplexed geologists for decades, is expected to be resolved.

MATERIALS AND METHODS

LROC WAC global mosaic

The geological background analysis of the CE-6 landing area is based on the global mosaic generated from the LROC wide-angle camera (WAC). The WAC is a push-frame camera with resolutions of 75 and 384 m (at an altitude of 50 km) in the visible and ultraviolet bands, respectively.[52] The LROC WAC image covers a swath ~104 km wide from the nominal 50 km orbit,[52] which allowed the instrument team to create a number of global mosaics with favorable quality. In this research, the WAC global mosaic created in June 2013 (Database: https://astrogeology.usgs.gov/search/map/Moon/LRO/LROC_WAC/Lunar_LRO_LROC-WAC_Mosaic_global_100m_June2013)[53,54] was used as the basemap for geological analysis of the CE-6 landing area. The locations of SPACA found by Moriarty and Pieters,[28] the impact melt area in the numerical simulation by Potter et al.,[27] and the Apollo craters along with the CE-6 landing site are all registered in the mosaic.

SLDEM2015 data

In this research, the lunar topographic data of SLDEM2015 are used to check our numerical simulation results. The data are generated by co-registering and combining SELENE Terrain Camera DEM with LRO laser altimetric data produced by Barker et al.,[55] and they are at the spatial resolution of 60 m/pixel. They are widely used in lunar scientific studies and can be freely downloaded from the Database: https://astrogeology.usgs.gov/search/map/Moon/LRO/LOLA/Lunar_LRO_LOLAKaguya_Shade_60N60S_512ppd.

Lunar gravity anomaly and crust thickness data

Lunar gravity data are obtained through the Gravity Recovery and Interior Laboratory (GRAIL) mission,[56] which is a spacecraft-to-spacecraft tracking mission aiming to produce a detailed map of the lunar gravity field. The Bouguer-corrected GRAIL gravity anomaly data used in this research are from the Database: https://pds-geosciences.wustl.edu/grail/grail-l-lgrs-5-rdr-v1/grail_1001/shadr/. The crustal thickness map of the Moon used in the research is derived from GRAIL gravity data by Wieczorek et al.,[57] and it was downloaded from the Database: https://zenodo.org/records/997347.

Mineral and elements distribution data

In this research, the TiO_2 abundance map of the Moon by Sato et al.[41] is used as the basemap to delineate the geological boundary of the CE-6 landing area. The product was derived from the ultraviolet and visible reflectance acquired by the LROC WAC and was often used in dividing the lunar basalt units.[58,59] The resolution of the product is ~400 m/pixel, and they are available from the Database: https://pds.lroc.asu.edu/data/LRO-L-LROC-5-RDR-V1.0/LROLRC_2001/DATA/SDP/WAC_TIO2/.

The abundance of FeO and major minerals of clinopyroxene, orthopyroxene, olivine, and feldspar were from the results by Lemelin et al.,[40] which were derived from the Kaguya Multiband Imager reflectance data. The resolutions of these products are ~60 m/pixel, and they are available from the Database: http://astrogeology.usgs.gov/pds/annex.

High-resolution imagery product

The high-resolution mosaic from the LROC NAC images is produced in this research as a basemap to extract and measure craters in the CE-6 landing area. The LROC NAC images cover most of the lunar surface with a resolution of 0.5–2 m and are currently the highest-resolution orbiter images. The LROC NAC images were downloaded from the PDS Geosciences Node Lunar Orbital Data Explorer website (Database: https://ode.rsl.wustl.edu/moon/index.aspx), and the detailed process for generating large-area digital orthophoto maps (DOM) can be found in Di et al.[60]

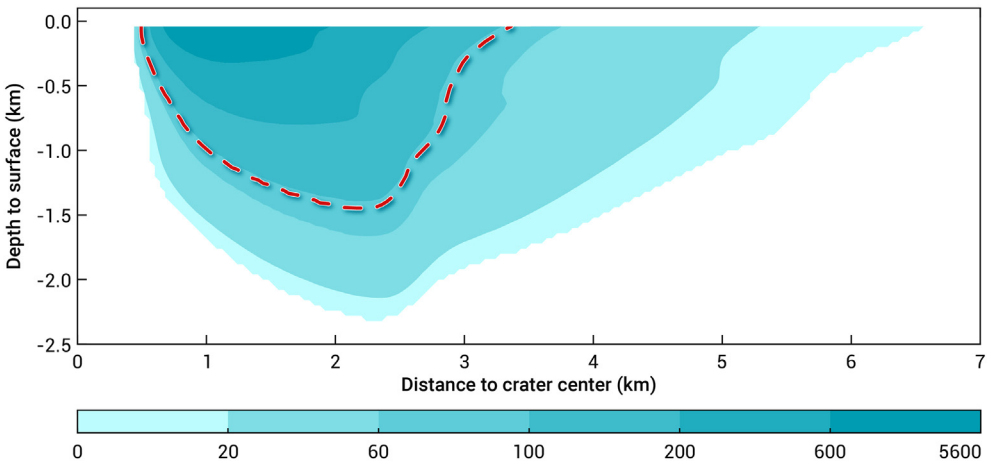

Figure 6. Ejected distance of the initial target material during the formation of the Chaffee S crater The horizontal and vertical axes represent the radial distance and depth from the impact point, respectively. Different colors indicate the sputtering distance of the target material (unit: km). The black dashed line represents the initial locations of the target material that might be ejected to the CE-6 landing site.

Crater mapping and analysis

To delineate the crater rim and measure the diameter, the high-resolution LROC NAC mosaic was integrated into the platform of ArcGIS, and the CraterTools toolkit[61] was used to manually map the craters. The CraterTools toolkit can measure the crater diameter correctly regardless of the map projection,[61] and it can work well with three points on the crater rims identified. When manually digitizing a crater, the three points on the crater rim should be as evenly distributed as possible, which can give the minimum error.[62]

The completeness diameter of the mapped crater catalog is analyzed with the program by Robbins et al.,[44] which is available at the website: https://github.com/CraterAnalysis/CraterAnalysis. To date the geological age of the CE-6 landing area with the mapped craters, the program Craterstats[63,64] is used in the research. In addition, the lunar crater chronology function by Yue et al.[18] and the production function by Neukum et al.[45] are used to derive the model age with the size-frequency distribution of the mapped craters.

To search for the potential source craters of the possible exotic material in CE-6 samples, young craters throughout the Moon were searched based on the crater catalog by Losiak et al.,[65] the geological map of the northern SPA basin by Ivanov et al.,[33] and the global lunar geological map by Fortezzo et al.[66] All the Copernican craters from the three crate datasets are considered as the potential source of the exotic material of CE-6 samples. Some Eratosthenian craters may also eject materials to the CE-6 landing area; however, they should be buried by the ejecta from subsequent Copernican craters. Despite the possibility that a small amount of Eratosthenian ejecta might be excavated to the shallow subsurface by later local bombardment, the likelihood of ejecta from an Eratosthenian impact crater being present in the CE-6 samples is small. This is because the CE-6 landing site is mainly surrounded by small impact craters, which have a very low excavation efficiency for lunar surface materials.[67] As a result, there are 253 craters being considered as the potential source of exotic material in the CE-6 sample.

Crater ejecta thickness analysis

The crater ejecta thickness is often used as a measurement to evaluate the probability of material presence from source craters.[21,68,69] However, there are currently several ways to evaluate the ejecta thickness. Based on the observations of nuclear craters, the terrestrial Meteor Crater, and lunar craters, McGetchin et al.[70] showed that the ejecta thickness on the crater rim is $T = 0.14R^{0.74}$ (unit: m), and it decreases exponentially with a power of −3 as the distance from the center of the crater increases. However, Pike[71] argued that there were only two lunar craters involved in the fitting, and he proposed three alternate models, although he admitted these models are subject to various uncertainties. Settle et al.[72] pointed out that two of the three models proposed by Pike[71] were actually quite close to his equation. Based on the classification of impact craters, Pike[73] further optimized the ejecta thickness models on the crater rim, and it was later inherited by Sharpton.[49] However, according to the interpretation of the rim height from high-resolution lunar orbital images, Sharpton[49] pointed out that only a fraction of the rim height is attributed to the ejecta thickness. In addition, Sharpton[49] also admitted that the ejecta thickness decreases exponentially with a power of −3 as the distance from the center of the crater increases. Finally, the combined empirical equations to calculate the ejecta thickness are as follows:

$$\delta = \begin{cases} 0.014R^{1.01}\left(\frac{r}{R}\right)^{-3.0}, 1.1\ \text{km} < R < 8.5\ \text{km} \\ 3.95R^{0.399}\left(\frac{r}{R}\right)^{-3.0}, 8.5\ \text{km} < R < 22.5\ \text{km} \end{cases} \quad \text{(Equation 1)}$$

where r is the distance from the crater center, R is the crater rim radius, and all dimensions are in meters. This model has been widely used in recent studies.[74–76]

Numerical simulation of Chaffee S crater

The formation process of the Chaffee S crater is simulated with the 2D version of the hydrocode SALEc,[77] which can be freely downloaded from the website: https://github.com/huachengli/SALEc-public. The most basic governing equations of the SALEc hydrocode include the conservation equations of the mass, momentum, and energy, along with the constitutive equations and equations of state for different geologically interesting materials. The hydrocode SALEc has been benchmarked by laboratory experiments and other hydrocodes in impact cratering simulations, and Li et al.[77] listed the details on the code.

In the simulations of the Chaffee S crater, the projectile is represented by dunite because it is a reasonable approximation of a typical ordinary chondrite asteroidal material,[78] and the target is represented by basalt according to the geological context of the Chaffee S crater. We varied the impact speed between 10 and 18 km/s, and adjusted the projectile diameter accordingly, to ensure that the simulated impact crater matches the observed results. The grid size of the model is 40 m, and there are 20 cells per projectile radius. The models along with the corresponding parameters for dunite and basalt are listed in Table S1. After more than 60 instances of trial and error, the best-fit model is found with a projectile diameter of 1.6 km and a velocity of 11 km/s. The profile of the crater wall in the numerical simulation results is very close to that in the remote sensing observations (Figure S5) except that the crater depth obtained from the numerical simulation (~3.9 km) is slightly deeper than the remote sensing observations (~3.4 km).

REFERENCES

1. Smith, J.V., Anderson, A.T., Newton, R.C., et al. (1970). Petrologic history of the moon inferred from petrography, mineralogy and petrogenesis of Apollo 11 rocks. In Paper Presented at Apollo 11 Lunar Science Conference, Houston, Texas, January 5-8, pp. 897–925.
2. Wood, J.A., Dickey, J.S., Jr., Marvin, U.B., et al. (1970). Lunar anorthosites and a geophysical model of the Moon. In Paper Presented at the Apollo 11 Lunar Science Conference, Houston, Texas, January 5-8, p. 965.
3. Hu, S., He, H., Ji, J., et al. (2021). A dry lunar mantle reservoir for young mare basalts of Chang'e-5. Nature ***600***(7887): 49–53. https://doi.org/10.1038/s41586-021-04107-9.
4. Stevenson, D.J. (1987). Origin of the Moon-The Collision Hypothesis. Annu. Rev. Earth Planet Sci. ***15***: 271–315. https://doi.org/10.1146/annurev.ea.15.050187.001415.
5. Canup, R.M. (2004). Simulations of a late lunar-forming impact. Icarus ***168***: 433–456. https://doi.org/10.1016/j.icarus.2003.09.028.
6. Chen, Y., Hu, S., Li, J.-H., et al. (2023). Chang'e-5 lunar samples shed new light on the Moon. Innovat. Geosci. ***1***(1): 100014. https://doi.org/10.59717/j.xinn-geo.2023.100014.
7. Yang, W., and Lin, Y. (2021). New Lunar Samples Returned by Chang'e-5: Opportunities for New Discoveries and International Collaboration. Innovation ***2***(1): 100070. https://doi.org/10.1016/j.xinn.2020.100070.
8. Wasson, J.T., and Warren, P.H. (1980). Contribution of the mantle to the lunar asymmetry. Icarus ***44***(3): 752–771. https://doi.org/10.1016/0019-1035(80)90142-6.
9. Stevenson, D.J. (1980). Lunar asymmetry and palaeomagnetism. Nature ***287***(5782): 520–521. https://doi.org/10.1038/287520a0.
10. Lucey, P.G., Blewett, D.T., and Hawke, B.R. (1998). Mapping the FeO and TiO_2 content of the lunar surface with multispectral imagery. J. Geophys. Res. ***103***(E2): 3679–3699. https://doi.org/10.1029/97JE03019.
11. Zhang, N., Ding, M., Zhu, M.-H., et al. (2022). Lunar compositional asymmetry explained by mantle overturn following the South Pole–Aitken impact. Nat. Geosci. ***15***(1): 37–41. https://doi.org/10.1038/s41561-021-00872-4.
12. Zhong, S., Parmentier, E.M., and Zuber, M.T. (2000). A dynamic origin for the global asymmetry of lunar mare basalts. Earth Planet Sci. Lett. ***177***(3): 131–140. https://doi.org/10.1016/S0012-821X(00)00041-8.
13. Liu, Z., Peng, M., Di, K., et al. (2024). High-precision visual localization of the Chang'e-6 lander. Natl. Rem. Sens. Bull. ***28***(6): 1649–1656. https://doi.org/10.11834/jrs.20244229.
14. Zeng, X., Liu, D., Chen, Y., et al. (2023). Landing site of the Chang'e-6 lunar farside sample return mission from the Apollo basin. Nat. Astron. ***7***: 1188–1197. https://doi.org/10.1038/s41550-023-02038-1.
15. Che, X., Nemchin, A., Liu, D., et al. (2021). Age and composition of young basalts on the Moon, measured from samples returned by Chang'e-5. Science ***374***(6569): 887–890. https://doi.org/10.1126/science.abl7957.
16. Li, Q.-L., Zhou, Q., Liu, Y., et al. (2021). Two-billion-year-old volcanism on the Moon from Chang'e-5 basalts. Nature ***600***(7887): 54–58. https://doi.org/10.1038/s41586-021-04100-2.
17. Tian, H.-C., Wang, H., Chen, Y., et al. (2021). Non-KREEP origin for Chang'e-5 basalts in the Procellarum KREEP Terrane. Nature ***600***(7887): 59–63. https://doi.org/10.1038/s41586-021-04119-5.
18. Yue, Z., Di, K., Wan, W., et al. (2022). Updated lunar cratering chronology model with the radiometric age of Chang'e-5 samples. Nat. Astron. ***6***: 541–545. https://doi.org/10.1038/s41550-022-01604-3.
19. Qian, Y.Q., Xiao, L., Zhao, S.Y., et al. (2018). Geology and Scientific Significance of the Rümker Region in Northern Oceanus Procellarum: China's Chang'E-5 Landing Region. JGR. Planets ***123***(6): 1407–1430. https://doi.org/10.1029/2018JE005595.
20. Jia, M., Yue, Z., Di, K., et al. (2020). A catalogue of impact craters larger than 200 m and surface age analysis in the Chang'e-5 landing area. Earth Planet Sci. Lett. ***541***: 116272. https://doi.org/10.1016/j.epsl.2020.116272.
21. Xie, M., Xiao, Z., Zhang, X., et al. (2020). The Provenance of Regolith at the Chang'e-5 Candidate Landing Region. JGR. Planets ***125***(5): e2019JE006112. https://doi.org/10.1029/2019JE006112.
22. Garrick-Bethell, I., and Zuber, M.T. (2009). Elliptical structure of the lunar South Pole-Aitken basin. Icarus ***204***(2): 399–408. https://doi.org/10.1016/j.icarus.2009.05.032.
23. Garrick-Bethell, I., Miljković, K., Hiesinger, H., et al. (2020). Troctolite 76535: A sample of the Moon's South Pole-Aitken basin? Icarus ***338***: 113430. https://doi.org/10.1016/j.icarus.2019.113430.
24. Petro, N.E., and Pieters, C.M. (2004). Surviving the heavy bombardment: Ancient material at the surface of South Pole-Aitken Basin. J. Geophys. Res. ***109***(E6): E06004. https://doi.org/10.1029/2003JE002182.
25. Ivanov, B.A. (2007). Lunar Impact Basins - Numerical Modeling. In Paper presented at 38th Lunar and Planetary Science Conference, League City, Texas, March 12-16, p. 2003.
26. Melosh, H.J., Kendall, J., Horgan, B., et al. (2017). South Pole–Aitken basin ejecta reveal the Moon's upper mantle. Geology ***45***(12): 1063–1066. https://doi.org/10.1130/g39375.1.
27. Potter, R.W.K., Collins, G.S., Kiefer, W.S., et al. (2012). Constraining the size of the South Pole-Aitken basin impact. Icarus ***220***(2): 730–743. https://doi.org/10.1016/j.icarus.2012.05.032.

28. Moriarty, D.P.III., and Pieters, C.M. (2018). The Character of South Pole-Aitken Basin: Patterns of Surface and Subsurface Composition. JGR. Planets ***123***(3): 729–747. https://doi.org/10.1002/2017JE005364.
29. Vaughan, W.M., and Head, J.W. (2014). Impact melt differentiation in the South Pole-Aitken basin: Some observations and speculations. Planet. Space Sci. ***91***: 101–106. https://doi.org/10.1016/j.pss.2013.11.010.
30. Baker, D.M., and Head, J.W. (2015). Constraints on the depths of origin of peak rings on the Moon from Moon Mineralogy Mapper data. Icarus ***258***: 164–180. https://doi.org/10.1016/j.icarus.2015.06.013.
31. Baker, D.M., Head, J.W., Fassett, C.I., et al. (2011). The transition from complex crater to peak-ring basin on the Moon: New observations from the Lunar Orbiter Laser Altimeter (LOLA) instrument. Icarus ***214***(2): 377–393. https://doi.org/10.1016/j.icarus.2011.05.030.
32. Hiesinger, H., van der Bogert, C., Pasckert, J., et al. (2012). New crater size-frequency distribution measurements of the South Pole-Aitken basin. In Paper Presented at 43rd Lunar and Planetary Science Conference, The Woodlands, Texas, March 19-23, p. 2863.
33. Ivanov, M.A., Hiesinger, H., van der Bogert, C.H., et al. (2018). Geologic History of the Northern Portion of the South Pole-Aitken Basin on the Moon. JGR. Planets ***123***(10): 2585–2612. https://doi.org/10.1029/2018JE005590.
34. Orgel, C., Michael, G.G., Fassett, C.I., et al. (2018). The Lunar Basin Sequence Based on Absolute Model Ages Derived via Buffered Non-Sparseness Correction: Implications for Impactor Population(s). In Paper Presented at 49th Lunar and Planetary Science Conference, The Woodlands, Texas, March 19–23, p. 1935.
35. Liu, J., Liu, J., Yue, Z., et al. (2022). Characterization and interpretation of the global lunar impact basins based on remote sensing. Icarus ***378***: 114952. https://doi.org/10.1016/j.icarus.2022.114952.
36. Baker, D.M., Head, J.W., Collins, G.S., et al. (2016). The formation of peak-ring basins: Working hypotheses and path forward in using observations to constrain models of impact-basin formation. Icarus ***273***: 146–163. https://doi.org/10.1016/j.icarus.2015.11.033.
37. Melosh, H.J. (1989). Impact Cratering: A Geologic Process (Oxford University Press).
38. Potter, R.W., Head, J.W., Guo, D., et al. (2018). The Apollo peak-ring impact basin: Insights into the structure and evolution of the South Pole–Aitken basin. Icarus ***306***: 139–149. https://doi.org/10.1016/j.icarus.2018.02.007.
39. Zhang, L., Zhang, X., Yang, M., et al. (2023). New maps of major oxides and Mg # of the lunar surface from additional geochemical data of Chang'E-5 samples and KAGUYA multiband imager data. Icarus ***397***: 115505. https://doi.org/10.1016/j.icarus.2023.115505.
40. Lemelin, M., Lucey, P.G., Gaddis, L.R., et al. (2016). Global map products from the Kaguya Multiband Imager at 512 ppd: Minerals, FeO and OMAT. In Paper Presented at 47th Lunar and Planetary Science Conference, The Woodlands, Texas, March 21–25, p. 2994.
41. Sato, H., Robinson, M.S., Lawrence, S.J., et al. (2017). Lunar mare TiO_2 abundances estimated from UV/Vis reflectance. Icarus ***296***: 216–238. https://doi.org/10.1016/j.icarus.2017.06.013.
42. Hiesinger, H., Jaumann, R., Neukum, G., et al. (2000). Ages of mare basalts on the lunar nearside. J. Geophys. Res. ***105***(E12): 29239–29275. https://doi.org/10.1029/2000JE001244.
43. Giguere, T.A., Taylor, G.J., Hawke, B.R., et al. (2000). The titanium contents of lunar mare basalts. Meteorit. Planet. Sci. ***35***(1): 193–200. https://doi.org/10.1111/j.1945-5100.2000.tb01985.x.
44. Robbins, S.J., Riggs, J.D., Weaver, B.P., et al. (2018). Revised recommended methods for analyzing crater size-frequency distributions. Meteorit. Planet. Sci. ***53***(4): 891–931. https://doi.org/10.1111/maps.12990.
45. Neukum, G., Ivanov, B.A., and Hartmann, W.K. (2001). Cratering records in the inner solar system in relation to the lunar reference system. Space Sci. Rev. ***96***: 55–86. https://doi.org/10.1023/A:1011989004263.
46. Michael, G.G., Kneissl, T., and Neesemann, A. (2016). Planetary surface dating from crater size-frequency distribution measurements: Poisson timing analysis. Icarus ***277***: 279–285. https://doi.org/10.1016/j.icarus.2016.05.019.
47. Michael, G.G., Platz, T., Kneissl, T., et al. (2012). Planetary surface dating from crater size–frequency distribution measurements: Spatial randomness and clustering. Icarus ***218***(1): 169–177. https://doi.org/10.1016/j.icarus.2011.11.033.
48. Qian, Y., Head, J., Michalski, J., et al. (2024). Long-lasting farside volcanism in the Apollo basin: Chang'e-6 landing site. Earth Planet Sci. Lett. ***637***: 118737. https://doi.org/10.1016/j.epsl.2024.118737.
49. Sharpton, V.L. (2014). Outcrops on lunar crater rims: Implications for rim construction mechanisms, ejecta volumes and excavation depths. JGR. Planets ***119***(1): 154–168. https://doi.org/10.1002/2013JE004523.
50. Jia, Z., Chen, J., Kong, J., et al. (2024). Geologic context of Chang'e-6 candidate landing regions and potential non-mare materials in the returned samples. Icarus ***416***: 116107. https://doi.org/10.1016/j.icarus.2024.116107.
51. Petro, N.E., Sunshine, J., Pieters, C., et al. (2010). Lower Crustal Materials Exposed in the Apollo Basin Revealed Using Moon Mineralogy Mapper (M^3) Data. In Paper Presented at 41st Lunar and Planetary Science Conference, The Woodlands, Texas, March 1-5, p. 1802.
52. Robinson, M.S., Brylow, S.M., Tschimmel, M., et al. (2010). Lunar Reconnaissance Orbiter Camera (LROC) instrument overview. Space Sci. Rev. ***150***: 81–124. https://doi.org/10.1007/s11214-010-9634-2.
53. Speyerer, E., Robinson, M., and Denevi, B. (2011). Lunar Reconnaissance Orbiter Camera global morphological map of the Moon. In Paper Presented at 42nd Lunar and Planetary Science Conference, The Woodlands, Texas, March 7-11, p. 2387.
54. Wagner, R.V., Speyerer, E.J., Robinson, M.S., et al. (2015). New Mosaicked Data Products from the LROC Team. In Paper Presented at 46th Lunar and Planetary Science Conference, The Woodlands, Texas, March 16–20, p. 1473.
55. Barker, M.K., Mazarico, E., Neumann, G.A., et al. (2016). A new lunar digital elevation model from the Lunar Orbiter Laser Altimeter and SELENE Terrain Camera. Icarus ***273***: 346–355. https://doi.org/10.1016/j.icarus.2015.07.039.
56. Zuber, M.T., Smith, D.E., Watkins, M.M., et al. (2013). Gravity Field of the Moon from the Gravity Recovery and Interior Laboratory (GRAIL) Mission. Science ***339***(6120): 668–671. https://doi.org/10.1126/science.1231507.
57. Wieczorek, M.A., Neumann, G.A., Nimmo, F., et al. (2013). The Crust of the Moon as Seen by GRAIL. Science ***339***(6120): 671–675. https://doi.org/10.1126/science.1231530.
58. Zhang, C., Chen, J., Pan, Y., et al. (2024). Geomorphology, Mineralogy, and Chronology of Mare Basalts in the Oceanus Procellarum Region. Rem. Sens. ***16***(4): 634. https://doi.org/10.3390/rs16040634.
59. Zhao, Z., Chen, J., Ling, Z., et al. (2023). Chronology, composition, and mineralogy of mare basalts in the junction of Oceanus Procellarum, Mare Imbrium, Mare Insularum, and Mare Vaporum. Icarus ***397***: 115531. https://doi.org/10.1016/j.icarus.2023.115531.
60. Di, K., Jia, M., Xin, X., et al. (2019). High-Resolution Large-Area Digital Orthophoto Map Generation Using LROC NAC Images. Photogramm. Eng. Rem. Sens. ***85***(7): 481–491. https://doi.org/10.14358/PERS.85.7.481.
61. Kneissl, T., van Gasselt, S., and Neukum, G. (2011). Map-projection-independent crater size-frequency determination in GIS environments—New software tool for ArcGIS. Planet. Space Sci. ***59***(11): 1243–1254. https://doi.org/10.1016/j.pss.2010.03.015.
62. Yue, Z., Di, K., Liu, Z., et al. (2019). Lunar regolith thickness deduced from concentric craters in the CE-5 landing area. Icarus ***329***: 46–54. https://doi.org/10.1016/j.icarus.2019.03.032.
63. Michael, G.G. (2013). Planetary surface dating from crater size–frequency distribution measurements: Multiple resurfacing episodes and differential isochron fitting. Icarus ***226***(1): 885–890. https://doi.org/10.1016/j.icarus.2013.07.004.
64. Michael, G.G., and Neukum, G. (2010). Planetary surface dating from crater size–frequency distribution measurements: Partial resurfacing events and statistical age uncertainty. Earth Planet Sci. Lett. ***294***(3): 223–229. https://doi.org/10.1016/j.epsl.2009.12.041.
65. Losiak, A., Wilhelms, D.E., Byrne, C.J., et al. (2009). A New Lunar Impact Crater Database. In Paper presented at 40th Lunar and Planetary Science Conference, The Woodlands, Texas, March 23-27, p. 1532. Revised by Öhman, T., Lunar and Planetary Institute & Arctic Planetary Science Institute (2011) and (2015). https://www.lpi.usra.edu/lunar/surface/Lunar_Impact_Crater_Database_v1508Sep2015.xls.
66. Fortezzo, C.M., Spudis, P.D., and Harrel, S.L. (2020). Release of the Digital Unified Global Geologic Map of the Moon At 1:5,000,000- Scale. In Paper presented at 51st Lunar and Planetary Science Conference, the Woodlands, Texas, March 16–20, p. 2760.
67. Shi, K., Yue, Z., Di, K., et al. (2022). The gardening process of lunar regolith by small impact craters: A case study in Chang'E-4 landing area. Icarus ***377***: 114908. https://doi.org/10.1016/j.icarus.2022.114908.
68. Jia, B., Fa, W., Xie, M., et al. (2021). Regolith Properties in the Chang'E-5 Landing Region of the Moon: Results From Multi-Source Remote Sensing Observations. JGR. Planets ***126***(7): e2021JE006934. https://doi.org/10.1029/2021JE006934.
69. Jia, B., Fa, W., Zhang, M., et al. (2022). On the provenance of the Chang'E-5 lunar samples. Earth Planet Sci. Lett. ***596***: 117791. https://doi.org/10.1016/j.epsl.2022.117791.
70. McGetchin, T.R., Settle, M., and Head, J.W. (1973). Radial thickness variation in impact crater ejecta: implications for lunar basin deposits. Earth Planet Sci. Lett. ***20***(2): 226–236. https://doi.org/10.1016/0012-821X(73)90162-3.
71. Pike, R.J. (1974). Ejecta from large craters on the Moon: Comments on the geometric model of McGetchin et al. Earth Planet Sci. Lett. ***23***(3): 265–271. https://doi.org/10.1016/0012-821X(74)90114-9.
72. Settle, M., Head, J.W., and McGetchin, T.R. (1974). Ejecta from large craters on the moon: Discussion. Earth Planet Sci. Lett. ***23***(3): 271–274. https://doi.org/10.1016/0012-821X(74)90115-0.
73. Pike, R.J. (1977). Size-dependence in the shape of fresh impact craters on the moon. In Impact and Explosion Cratering: Planetary and Terrestrial Implications (Proceedings of the Symposium on Planetary Cratering Mechanics, Flagstaff, Arizona, September 13-17, 1976), D.J. Roddy, R.O. Pepin, and P.B. Merrill, eds. (Pergamon Press, Inc.), pp. 489–509.
74. Wang, X., Head, J.W., Chen, Y., et al. (2024). Lunar Farside South Pole-Aitken Basin Interior: Evidence for More Extensive Central Cryptomaria in the South Pole-Aitken Compositional Anomaly (SPACA). JGR. Planets ***129***(5): e2023JE008176. https://doi.org/10.1029/2023JE008176.
75. Krasilnikov, A.S., Krasilnikov, S.S., Ivanov, M.A., et al. (2023). Estimation of Ejecta Thickness from Impact Craters in the South Polar Region of the Moon. Sol. Syst. Res. ***57***(2): 122–132. https://doi.org/10.1134/S0038094623020041.
76. Rajasekhar, R.P., Dagar, A.K., Nagori, R., et al. (2024). Comprehensive analysis of Chandrayaan-3 landing site region focussing on morphology, hydration and gravity anomalies. Icarus ***415***: 116074. https://doi.org/10.1016/j.icarus.2024.116074.
77. Li, H., Yue, Z., Lin, Y., et al. (2023). Olivine origination in lunar Das crater through three-dimensional numerical simulation. Icarus ***391***: 115333. https://doi.org/10.1016/j.icarus.2022.115333.
78. Silber, E.A., Osinski, G.R., Johnson, B.C., et al. (2017). Effect of impact velocity and acoustic fluidization on the simple-to-complex transition of lunar craters. JGR. Planets ***122***(5): 800–821. https://doi.org/10.1002/2016JE005236.

ACKNOWLEDGMENTS

This study was supported by the National Key Research and Development Program of China (grant no. 2022YFF0503100), the B-type Strategic Priority Program of the Chinese Academy of Sciences (grant no. XDB41000000), the Open Fund of the State Key Laboratory of Remote Sensing Science (grant no. OFSLRSS202206), the National Natural Science Foundation of China (grant no. 62227901), and the key research program of the Institute of Geology and Geophysics, Chinese Academy of Sciences (grant no. IGGCAS-202401, IGGCAS-202204).

AUTHOR CONTRIBUTIONS

Z.Y., S.G., W.Y., Y.L., X.L., and F.W. conceived the study. Z.Y., S.G., H.L., and Y.C. analyzed the geological background. Z.Y., S.S., Y.W., and K.D. processed the data and mapped all the craters for surface dating. Z.Y. carried out the numerical simulation of the Chaffee S crater. Z.Y. wrote the initial draft of the manuscript, and all authors contributed to subsequent revisions.

DECLARATION OF INTERESTS

The authors declare no competing interests.

SUPPLEMENTAL INFORMATION

It can be found online at https://doi.org/10.1016/j.xinn.2024.100663.

LEAD CONTACT WEBSITE

https://igg.cas.cn/sourcedb_igg_cas/cn/zjrck/yjy/202206/t20220613_6460446.htm.